Generation of an allelic series at the *Ahr* locus using an Edited Recombinant Approach

Wilson, R. H.[1,2], Carney, P. R.[1,2], Glover, E.[2], Parrott, J. C.[1,2], Rojas, B. L. [1,2], Moran, S. M.[2], Yee, J. S.[1,2], Nukaya, M.[1], Goetz, N. A.[2], Rubenstein, C. D.[3], Krentz, K. J.[3], Xing, Y. [1,2], and Bradfield, C. A.[1,2,3]

[1] Molecular and Environmental Toxicology Center, University of Wisconsin- Madison, Madison, WI
[2] Department of Oncology, School of Medicine and Public Health, University of Wisconsin-Madison, Madison, WI
[3] Biotechnology Center, University of Wisconsin- Madison, Madison, WI

Address correspondence to:

Christopher A. Bradfield, Ph.D.
McArdle Laboratory for Cancer Research
School of Medicine and Public Health
University of Wisconsin - Madison
1400 University Avenue
Madison, WI 53706

ABSTRACT

The aryl hydrocarbon receptor (AHR) is a ligand activated transcription factor and a member of the PER-ARNT-SIM (PAS) superfamily of environmental sensors. The AHR is involved in a series of biological processes including adaptive metabolism of xenobiotics, toxicity of certain environmental pollutants, vascular development, fertility, and immune function. Mouse models, including the *Ahr* null and *Ahr* conditional null mice, are widely used for the study of AHR-mediated biology and toxicity. The *Ahr* conditional null mouse harbors the low affinity Ahr^{d} allele that exhibits approximately a 10-fold lower binding affinity for AHR ligands than the widely used C57BL/6 mouse that harbors the higher affinity Ahr^{b1} allele. Here, we report a novel mouse model that introduces a V375A polymorphism that converts the low affinity allele into a high-affinity allele, offering a more sensitive conditional model. In the generation of this novel conditional allele, two additional mutants arose, including a three base pair deletion in the PAS-B domain (Ahr^{NG367R}) and an early termination codon in the PAS-B domain (Ahr^{Ter383}). The Ahr^{NG367R} allele presents as a phenocopy of the null and the Ahr^{Ter383} allele presents as an antimorph when assessing for the *ductus venosus* endpoint. These new models represent a series of tools that will be useful in further characterizing AHR biology.

Impact Statement: We describe the generation of three novel conditional mutations at the *Ahr* locus in mice. These include: a high affinity allele, a novel null allele, and an antimorphic allele. We propose these mutants will serve as powerful new tools for the study of chemicals that act through the AHR pathway.

INTRODUCTION

The aryl hydrocarbon receptor (AHR) is a ligand activated basic helix-loop-helix (bHLH) transcription factor that is a member of the PER-ARNT-SIM (PAS) superfamily of environmental sensors (McIntosh et al. 2010). The AHR is highly conserved in Chordates, though variation in receptor activity, sequence, and size is common (Hahn 2002; Poland et al. 1991). The naturally occurring *Ahr* polymorphisms in mice were essential tools in the discovery and characterization of the receptor (Ema et al. 1994; Nebert and Gelboin 1969; Poland and Glover 1975; 1980; Poland et al. 1976; Poland et al. 1994). For example, the differential response to polycyclic aromatic hydrocarbons across polymorphic strains contributed to the receptor's discovery (Nebert et al. 1975; Poland and Glover 1980; 1990; Poland et al. 1994). Subsequent characterization studies uncovered a prominent role for the AHR in upregulating genes, such as the cytochromes P450, that are responsible for metabolism of many of the receptor's ligands (Dragin et al. 2008). More recent studies have unveiled a role for the AHR in proper development of the vasculature as well as maintenance of the immune response at barrier tissues (Baricza et al. 2016; Bhaumik and Basu 2017; Haas et al. 2016; Harstad et al. 2006; Kiss et al. 2011; Lahvis et al. 2005; Metidji et al. 2018; Quintana et al. 2008; Veldhoen et al. 2008).

Decades of AHR research have yielded many different mouse models in efforts to answer important questions in AHR biology. Among these models is the conditional *Ahr* mouse (Ahr^{fx}) that allows cell specific deletion when crossed to transgenic lines expressing *Cre* recombinase in a cell specific manner (Walisser et al. 2005). While much has been learned from this model, the Ahr^{fx} allele was derived from 129-SvJ embryonic stem cells (ESCs) which harbor the less sensitive Ahr^{d} allele (Poland et al. 1994). The resultant lack of sensitivity to many xenobiotic ligands arising from this allele makes it difficult to characterize the cell-autonomous role of the AHR for certain endpoints. For example, to induce endpoints of interest, study of 2,3,7,8-tetrachlorodibenzo-*p*-dioxin (TCDD) toxicity requires significantly

higher doses in *Ahr*^{d} mice as compared to *Ahr*^{b} mice (*e.g.*, hepatocellular toxicity, hepatocellular carcinoma, and cleft pallet) (Kennedy et al. 2014). To improve this limitation, we selectively modified the ligand binding domain of the AHR in the existing *Ahr*^{fx} model to convert the low affinity residue V375 to the high affinity A375 (generating the *Ahr*^{V375A} allele) (Ema et al. 1994; Poland et al. 1994; Xing et al. 2012). To this end, we employed an "Edited Recombinant Approach" (ERA) to introduce a modification into the existing *Ahr*^{fx} allele using CRISPR-Cas9 (Ran et al. 2013; Sander and Joung 2014). The ERA allows enhancement of previously generated conditional alleles while limiting the technical challenges associated with generating multiple independent mutations in series.

In addition to the high affinity conditional allele (*Ahr*^{V375A}), we describe two additional alleles, an antimorphic allele and a novel null allele, generated serendipitously through the ERA that may also prove useful in our attempts to understand various aspects of AHR biology (*Ahr*^{NG367R} and *Ahr*^{Ter383}). To characterize each allele and understand the consequences of each mutation on AHR biology, we examined their influence on characteristic AHR-dependent phenotypes. These endpoints included the transcriptional responsiveness of these *Ahr* alleles to the nontoxic anthropogenic AHR ligand beta-naphthoflavone (βNF), the prevalence of the *ductus venosus* (DV) , and the response to the chemical colitigen dextran sodium sulfate (DSS) (Avilla et al. 2020; Díaz-Díaz et al. 2016; Furumatsu et al. 2011; Harstad et al. 2006; Lahvis et al. 2000; Lahvis et al. 2005; Nebert and Gelboin 1969; Poland and Glover 1975). Finally, we examined the cell autonomy of AHR signaling to determine if these mutant proteins function in the same cell-specific manner as the wildtype receptor. We propose that each of these alleles has utility and are important new members of an allelic series at the *Ahr* locus (Bunger et al. 2008; Bunger et al. 2003; Schmidt et al. 1996; Walisser et al. 2004a; Walisser et al. 2004b; Walisser et al. 2005).

MATERIALS AND METHODS

Guide RNA preparation: Two guide RNAs were designed for the generation of the *Ahr*^{V375A} conditional model to target the ligand binding domain in exon-7 of the *Ahr* gene. Guide DNA oligonucleotides were synthesized into a forward primer (5' GAAATTAATACGACTCACTATAGGN18-20**GTTTTAGAGCTAGAAATAGC** 3') which includes the desired target site and overlap (designated in bold) with the reverse primer (5' AAAAGCACCGACTCGGTGCCACTTTTTCAAGTTGATAACGGACTAGCCTTATTTTAACTT**GCTATTTCTAGCTCTAA AC** 3') which contains the sequence for the sgRNA stem loop structure necessary for incorporation into Cas9 (IDT, Coralville, IA) (Mali et al. 2013). The underlined nucleotides denote region where specific guide sequences are incorporated. Two guide sequences were used in the generation of these mice. Guide #1 sequence: **CCA**agtcacgcttgatttacagaaatg; guide sequence #2: **CCA**gattacatcatcgtcactca. Guide DNA was generated through PCR using Phusion High-Fidelity DNA Polymerase (New England BioLabs, Ipswich, MA). Guide DNA was run on a 1% agarose gel (124 base pairs) and purified (Macherey-Nagel, Duren, Germany). Approximately 100 ng of purified PCR product was used as a template for sgRNA synthesis using the T7 Megashortscript kit according to manufacture protocol (Ambion, Austin, TX). Following an *in vitro* transcription reaction, guide RNA was purified using MegaClear (Ambion, Austin, TX) and resuspended in injection buffer (Transgenic Animal Facility, UW-Madison, Madison, WI) at 100 ng/uL.

Generation of the conditional *Ahr*^{V375A} mouse model using CRISPR gene editing: To generate mice conditional for a high affinity ligand binding domain, three-week-old *Ahr*$^{fx/fx}$ dams (congenic on the B6 background for over 20 generations) were superovulated using Pregnant Mare Serum Gonadotropin (ProSpec Bio, East Brunswick, NJ) and human chorionic gonadotropin (Sigma-Aldrich, St. Louis, MO). Dams were then mated to *Ahr*$^{fx/fx}$ males to create homozygous *Ahr*$^{fx/fx}$ embryos. Day 0.5 embryos were

collected by the UW Genome Editing and Animal Models core and were microinjected with 50ng/ul guide RNA, 50ng/ul single stranded oligodeoxynucleotide (ssODN), and 40 ng/ul Cas9 protein (PNA Bio, Newbury Park, CA). Injected eggs were transplanted into pseudopregnant B6D2F1 females. Pups were sequenced at weaning to screen for gene edits. The ssODN targets the noncoding strand and encodes the sequence is 5'-GTGTAAGAAGACTTATGAAAACACAAACGCAGGACATGTTCTTTTTCTGATGCTTACGTCAGTGGTCTCTGAGTG**g**CGATGAT**a**TAATCTGGTCTTCCATTTCTGTAAATCAAGCGTGCATTGGACTGGACCCACCTCCAGCGACTGTGTTTTGCAAGA-3' where the lowercase bolded letters denote point mutations. The first point mutation changes codon 375 from GAC to GGC, whereas the second point mutation is a silent mutation introduced to disrupt the targeted cut site to prevent subsequent cleavage and indel formation in the ssODN.

Screening for CRISPR events: To characterize gene editing events, genomic DNA from the tails of resultant mice were sequenced. Genomic DNA was amplified using OL8165 (5'-GTACTGTACTGTACTGATGG - 3') and OL8166 (5'- CAGGTTCCATTGCCTTAGG - 3') which flank the region of *Ahr* targeted by the guide RNAs described above. The gene region of interest was amplified using PCR and OL 8165 and OL 8166. The PCR products were run on a 1% agarose gel to ensure presence of product at ~300 base pairs. The PCR product was cleaned up using Exo-SAP IT according to manufacturer's protocol (Applied Biosystems, Foster City, CA). In order to distinguish the sequences of each allele, the PCR products were cloned into pGEM-T Easy vector (Promega, Madison, WI). Ten successfully transformed colonies (as indicated visually by the blue/white screen intrinsic to the pGEM-T Easy vector) were sequenced. Sanger Sequencing experiments were performed by the DNA Sequencing Core at UW-Madison. Results were analyzed using FinchTV (Digital World Biology, Seattle, WA).

Animal care and treatment: Mice were housed in a selective pathogen-free facility in cages with corncob bedding. Mice had access to a chow diet and water *ad libitum* in accordance with the animal care protocol #M005987 approved by the University of Wisconsin Medical School's Animal Care and Use Committee. The *Ahr* null mice ($Ahr^{-/-}$) and Ahr^{fx} mice used in these studies were previously backcrossed to C57BL/6J (B6) mice (Jackson Laboratories, Bar Harbor, ME) for over 20 generations. The Ahr^{fx} mouse was the parental strain for the CRISPR-mediated mutations. The three CRISPR strains, Ahr^{V375A}, Ahr^{NG367R}, and Ahr^{Ter383}, were backcrossed onto B6 at least five times to eliminate off target effects for experiments (Aryal et al. 2018). For induction experiments, mice were treated with 80 ug/kg body weight of βNF (Sigma Aldrich, St. Louis, MO) dissolved in corn oil by oral gavage. Control animals receive 1mL/10 grams of body weight of corn oil alone by oral gavage. Mice are euthanized 4 hours following treatment via CO_2 inhalation. A section of the left lobe of the liver was collected immediately following euthanasia and placed in RNA*later* Stabilization Solution (Sigma Aldrich, St. Louis, MO). Mice used in induction studies were between 8-10 weeks old in age. Each group contains roughly equal numbers of males and females.

Western Blot: Western blots were performed on cytosolic fractions prepared from freshly harvested adult mouse liver, as described previously (LaPres et al. 2000). Protein samples were run on Mini-Protean TGX Stain-free gel (Bio-Rad Laboratories, Hercules, CA) transferred to PVDF membrane, and incubated overnight with the BEAR-3 antibody (1ug/mL; raised against amino acids 1-402 of AHR^{b1}) in 5% Blotto (non-fat dry milk in PBS), followed by 1 hour incubation in goat anti-Rabbit secondary antibody (Cat no. NB120-6024, Novus Biologics, Littleton, CO) in 5% Blotto. Blot was developed in alkaline phosphatase substrate 5-bromo-4-chloro-3-indolyl phosphate (BCIP) with nitroblue tetrazolium (NBT) for 8 minutes. The BEAR3 antibody was generated as described previously (Pollenz et al. 1994).

***Ductus venosus* scoring and liver lobe weights:** Prevalence of the DV was measured using gravity flow perfusion of the liver with trypan blue as described previously (Walisser et al. 2004a). Liver lobe weights were measured as previously described (Harstad et al. 2006). Briefly, livers were removed, and lobes were separated with scissors or razor blade. Each lobe (left, median, and rest) was weighed individually. The ration of left: median lobe was calculated by dividing the weight of the left lobe by that of the median lobe. Mice examined for DV and LLW were between 8-12 weeks old in age. Each group contains roughly equal numbers of males and females. Statistical differences were calculated using one-way ANOVA and deemed significant in cases where $p < 0.05$.

Dextran Sodium Sulfate treatment: Animals were given freshly prepared dextran sodium sulfate (DSS) (36,000-50,000 Da) diluted into acidified water from the animal facility at a concentration of 1% (MP Biomedicals, Irvine, CA) for five days as described previously (Díaz-Díaz et al. 2016). Mice were sacrificed on day five of DSS treatment. Colon was removed from each animal, cleaned with PBS, and measured from distal colon (following removal of the anus and rectum) to the proximal colon. Whole colon was saved in RNA later, as described below.

Cell specific excision: The $Ahr^{b1/V375A}$ heterozygous mice or $Ahr^{b1/Ter383}$ heterozygous mice were crossed to B6 mice harboring *Cre* recombinase transgenes under control of the *Albumin* (*Alb*; hepatocyte) or VE-Cadherin 5 (*Cdh5*; endothelial) promoter (Cre^{Alb} or Cre^{Cdh5}, respectively) (Jackson Laboratory) (Alva et al. 2006; Postic et al. 1999; Walisser et al. 2005). For the genotyping of the *Cre* recombinase transgene and the low affinity conditional *Ahr* allele, we used the JAX protocols (Jackson Laboratory) (Walisser et al. 2005). For the detection of the CRISPR-mediated mutations, we employed the Sanger sequencing method described above. In all cases, *Cre* negative littermates were used as controls to *Cre* positive

animals. In some experiments, mice were genotyped using commercial services that employ quantitative real time PCR (Transnetyx, Cordova, TN).

RNA isolation and Quantitative Real Time PCR (qPCR): Total RNA was isolated from liver and colon using Qiazol (Qiagen, Hilden, Germany) and the RNeasy Mini Kit (Qiagen. Hilden, Germany) according to manufacturer's protocol. The qPCR was performed as described previously (Baker et al. 2016). The reverse transcription reaction was completed using the High-Capacity cDNA Reverse Transcription Kit according to manufacturer's protocol (Thermo Fisher, Waltham, MA) with 1 ug of RNA starting material as a template for this reaction. The qPCR reaction was completed using the Quantstudio 7 Flex Real-Time PCR System (Thermo Fisher, Waltham, MA). The probes used include *Hprt* (Mm03024075_m1), *Cyp1a1* (Mm00487218_m1), *Cyp1a2* (Mm00487224_m1), *Cyp1b1*, and *Ahrr* (Mm01352370_m1) (Thermo Fisher, Waltham, MA). Relative expression was calculated in relation to *Hprt* expression.

Protein Modeling: Predicted AHR structures were visualized through PyMOL v 4.60. The PAS-B domain of AHR^{b1} shown was modeled and artificially colored in PyMOL using the protein model described previously (Xing et al. 2012).

Statistical Analysis: Statistics were performed using GraphPad Prism version 8.3.1 for Windows (GraphPad Software, La Jolla, CA). For gene induction data, groups were compared using a two-way ANOVA with multiple comparisons of the means (Tukey's Multiple Comparison Test). For DV and LLW analysis, groups were compared using a Chi-square (Fisher's exact test) or one-way ANOVA, respectively. The differences between groups were considered statistically significant when the p value was < 0.05. In figures, groups sharing a superscript are not statistically different. Statistically significant differences are marked by different superscripts. All experiments contain both male and female mice in each group.

RESULTS

Generation of an allelic series at *Ahr*: To generate mice harboring a high affinity conditional allele, Ahr^{fx} dams were mated to males of the same genotype to generate homozygous embryos. Embryos were harvested from pregnant females and microinjected with a guide RNA targeting the ligand binding domain in exon-7, Cas9 protein, and an ssODN containing the desired mutation. The injected embryos were then transferred to a pseudo-pregnant female and pups were screened for CRISPR events at weaning. Use of guide #1 yielded one CRISPR event in one mouse, resulting in a three base pair deletion that spans codons 367 and 368 (Ahr^{NG367R}) (Figure 1A, 2B). Use of guide #2 yielded two CRISPR events in one mouse on separate chromosomes (Figure 1B). The first event was a single adenine insertion at residue 371 resulting in a frame shift and early termination at residue 383 (Ahr^{Ter383}) (Figure 2C). The second event incorporates the ssODN to encode the high affinity alanine at residue 375 and a silent mutation seven base pairs downstream (Ahr^{V375A}) (Figure 2A). To separate these two events into distinct lines, the female founder was crossed to a B6 male. To confirm the segregation of alleles, F1s were sequenced. Each F1 mouse harbored the Ahr^{b1} allele (the B6 paternal allele) and either the *V375A* allele or the *Ter383* allele (the CRISPR'ed maternal allele). To eliminate potential off target CRISPR events, each line was backcrossed to B6 at least five times before being employed in an experiment (Aryal et al. 2018).

Protein expression in Ahr^{V375A}, Ahr^{NG367R}, and Ahr^{Ter383} mice: The three mutant alleles generated protein of the appropriate predicted size as recognized by an antibody (BEAR-3) raised against amino acids 1-402 of AHR^{b1} (Figure 3). Because proteins of different sizes transfer at different rates from polyacrylamide gel upon electrotransfer to PVDF membranes, the proteins were not quantified. Rather, the western blot was employed as a qualitative measure of protein size and its similarity to that predicted by the corresponding mutations described above.

***Ductus Venosus* phenotype of Ahr^{V375A}, Ahr^{NG367R}, and Ahr^{Ter383} mice:** Wildtype B6 mice ($Ahr^{b1/b1}$) and $Ahr^{fx/fx}$ mice developed with normal DV closure by early adulthood (n = 0/8 and n = 0/12, respectively) (Table 2A). Similarly, mice heterozygous for the Ahr^{b1} allele and the high affinity conditional allele (*i.e.*, $Ahr^{b1/V375A}$) and mice homozygous for the high affinity conditional allele ($Ahr^{V375A/V375A}$), also did not exhibit patent DV (n = 0/9 and n = 0/10, respectively) (Table 2A). In mice homozygous for the three base pair deletion allele ($Ahr^{NG367R/NG367R}$), the DV was patent at a prevalence of 100% (n = 13/13) (Table 2B). Mice heterozygous for this allele (*i.e.* $Ahr^{b1/NG367R}$) exhibited normal DV closure (n = 0/11) (Table 2B). For comparison, mice homozygous for the Ahr^{b1} allele did not display patent DV (n = 0/6) while mice homozygous for the null allele ($Ahr^{-/-}$) consistently exhibited patent DV (n = 15/15) (Table 2B). Mice homozygous for the truncated allele ($Ahr^{Ter383/Ter383}$) also exhibited 100% DV patency (n = 9/9) (Table 2C). Interestingly, mice heterozygous for the *b1* and *Ter383* allele ($Ahr^{b1/Ter383}$) exhibited patent DV with 85% penetrance (n = 16/19) compared to 100% of *Ahr* null animals (n = 15/15) (Table 2C). Haploinsufficient mice ($Ahr^{b1/-}$), as well as homozygous $Ahr^{b1/b1}$ mice, did not exhibited patent DV (n = 0/13 and n = 0/10, respectively) (Table 2C).

Liver lobe weights of Ahr^{V375A}, Ahr^{NG367R}, and Ahr^{Ter383} mice: To further characterize the consequences of each mutation on an additional AHR-mediated developmental phenotype, liver lobes were weighed. Wildtype B6 $Ahr^{b1/b1}$ mice, $Ahr^{fx/fx}$ mice, and $Ahr^{V375A/V375A}$ mice exhibited normal ratios of left to median lobe weights (Table 3). In $Ahr^{-/-}$, $Ahr^{NG367R/NG367R}$, and $Ahr^{b1/Ter383}$ mice, the left to median liver lobe weights were significantly decreased in comparison to wildtype counterparts ($p < 0.0001$) (Table 3).

Transcription of AHR-driven genes in the liver of Ahr^{V375A}, Ahr^{NG367R}, and Ahr^{Ter383} mice: To assess the consequences of the three mutations in the *Ahr* on expression of characteristic AHR-driven genes, we

measured hepatic mRNA transcript levels of *Cyp1a1*, *Cyp1a2*, *Cyp1b1,* and *Ahrr* from mice following a four-hour treatment with the AHR agonist βNF or the corn oil vehicle. Mice homozygous for the high affinity conditional allele ($Ahr^{V375A/V375A}$) were compared to wildtype ($Ahr^{b1/b1}$) and low affinity conditional ($Ahr^{fx/fx}$) counterparts (Figure 4). Mice with the high affinity conditional allele ($Ahr^{V375A/V375A}$) displayed a greater response (2.6 - 9.6 fold higher) for all transcripts compared to $Ahr^{fx/fx}$, which harbors V375. For example, induction of *Cyp1a1* was 9.6 times higher in $Ahr^{V375A/V375A}$ than in $Ahr^{fx/fx}$ mice, with a p value = 0.0002. Induction of *Cyp1a2* and *Cyp1b1* was 2.6 and 3.6 times higher, respectively, in $Ahr^{V375A/V375A}$ than in $Ahr^{fx/fx}$ mice (p value < 0.0001). Induction of *Ahrr* was 8 times higher in $Ahr^{V375A/V375A}$ than in $Ahr^{fx/fx}$ mice (p < 0.0001). Mice homozygous for the three base pair deletion ($Ahr^{NG367R/NG367R}$) were unresponsive compared to their high affinity conditional allele ($Ahr^{V375A/V375A}$) counterparts for induction of AHR target genes (Figure 5). The $Ahr^{NG367R/NG367R}$ mice were significantly (p < 0.001) less inducible (198, 6, 5.5, and 7.2 times, respectively) for *Cyp1a1*, *Cyp1a2*, *Cyp1b1*, and *Ahrr* than Ahr^{V375A} mice. Mice heterozygous for the truncated allele ($Ahr^{b1/Ter383}$) were less responsive to AHR-driven gene induction compared to wildtype ($Ahr^{b1/b1}$) but comparable to haploinsufficient ($Ahr^{b1/-}$) controls (Figure 6). The B6 wildtype controls ($Ahr^{b1/b1}$) were slightly more inducible for *Cyp1a1* (1.7 times), *Cyp1a2* (1.2 times), and *Cyp1b1* (1.6 times) than $Ahr^{b1/Ter383}$ counterparts, but these differences did not attain significance. The B6 wildtype controls are 7.3 times more inducible for *Ahrr* expression than the $Ahr^{b1/Ter383}$ mice. The haploinsufficient controls ($Ahr^{b1/-}$) and the $Ahr^{b1/Ter383}$ mice displayed similar induction of target genes.

Hepatocyte-specific excision of Ahr^{V375A} reduced expression of AHR-driven genes in liver but did not affect DV closure: To ensure conditionality of the Ahr^{V375A} allele, we crossed mice harboring this allele with mice harboring Cre^{Alb}. Mice from the F2 generation homozygous for Ahr^{V375A} with and without Cre^{Alb} were treated with βNF. After four hours, liver mRNA transcript levels of AHR-driven genes were measured. In Cre^{Alb} positive mice treated with βNF, gene expression of *Cyp1a1* and *Cyp1a2* were

markedly reduced ($p < 0.004$) (Figure 7). Expression of *Ahrr* and *Cyp1b1* was not significantly reduced in Cre^{Alb} positive Ahr^{V375A} mice. Excision of Ahr^{V375A} in hepatocytes ($Ahr^{V375A}Cre^{Alb}$) did not result in a patent DV (n = 0/10) (Table 4).

Endothelial specific deletion of Ahr^{V375A} was a vascular phenocopy of the *Ahr* null mouse: To determine if the Ahr^{V375A} mouse displayed the same cell autonomy as the Ahr^{fx} mouse characterized previously, we measured DV prevelence in Ahr^{V375A} mice crossed to mice harboring the *Cdh5*-driven *Cre* recombinase transgene (Alva et al. 2006; Walisser et al. 2005). Excision of Ahr^{V375A} in the endothelial compartment ($Ahr^{V375A}Cre^{Cdh5}$) resulted in a patent DV (n = 10/10) (Table 4).

Endothelial cell autonomy of Ahr^{Ter383} is a vascular phenocopy of the *Ahr* null mouse: Based upon the presence of patent DV in heterozygous Ahr^{Ter383} mice ($Ahr^{b1/Ter383}$), we postulated this allele was an antimorph in endothelial cells. To test this idea, we deleted the Ahr^{Ter383} allele in endothelial cells of heterozygous mice through a cross to a mouse carrying Cre^{Cdh5}. Prevalence of the patent DV was measured in mice globally heterozygous for the Ahr^{Ter383} construct but excised in *Cdh5*+ endothelial cells ($Ahr^{b1/Ter383}Cre^{Cdh5}$) (Table 5). In mice with the Ahr^{Ter383} construct removed in endothelial cells ($Ahr^{b1/Ter383}Cre^{Cdh5}$), we observed patent DV in 19% of mice (n = 2/11) compared to 86% patent DV in littermates that expressed Ahr^{Ter383} ubiquitously ($Ahr^{b1/Ter383}$, but with no Cre^{Cdh5}) (n = 19/22) (Table 5).

Heterozygous $Ahr^{b1/Ter383}$ response to chemically induced colitis: To determine if the Ahr^{Ter383} allele exhibited antimorphic properties for the chemically induced colitis endpoint as determined by colon length and induction of interleukin-1β (IL1β), mice were treated with DSS for five days. For both endpoints, the response of DSS treated $Ahr^{b1/Ter383}$ mice was similar to that observed in $Ahr^{b1/b1}$ wildtype mice, despite observing an enhanced response in $Ahr^{-/-}$ mice (Figure 8).

Structural Predictions: The PAS-B domain of the AHR^{b1} was modeled from that previously described (Figure 9) (Xing et al. 2012). Residues relevant for the three mutants were highlighted using Pymol (Xing et al. 2012).

DISCUSSION

The ERA described in this report employs the CRISPR-Cas9 technique to generate targeted mutations in a mouse line that has previously undergone a recombination event via gene targeting. This approach was initiated to improve the previously generated *Ahr*^{fx} allele by increasing the ligand binding affinity of the receptor product while maintaining the conditionality of the allele. To this end, we used CRISPR-Cas9 gene editing technology to generate the *Ahr*^{V375A} mouse by inducing the V375A codon change (Figure 1) (Adli 2018; Ceccaldi et al. 2016; Ran et al. 2013; Sander and Joung 2014; Singh et al. 2015). In this process, we observed neighboring recombination events in separate lines that were reflective of non-homologous end joining repair (NHEJ). The apparent NHEJ mechanism, which can occur at a higher frequency than HDR, generated two serendipitous mutations in codons near 375, yielding the *Ahr*^{NG367R} and *Ahr*^{Ter383} alleles (Figure 2). In this report, we provide an initial characterization of the three *Ahr* alleles in order to make them broadly available for developmental and toxicological studies.

The role of the AHR is highly context dependent, such that its biological outputs differ depending on the type of ligand, concentration of ligand, developmental stage, and cell type in which signaling occurs (Avilla et al. 2020; Cella and Colonna 2015; Esser 2016; Esser and Rannug 2015; Harrill et al. 2013; Larigot et al. 2018; Nebert 2017; Stevens et al. 2009). Previous studies have begun to unravel this complicated and differential biology using the conditional null model, commonly known as *Ahr*^{fx} (Villa et al. 2017; Walisser et al. 2005). The importance of cell type can be clearly shown as TCDD-induced hepatocellular toxicity is dependent upon AHR expression in hepatocytes, whereas AHR expression in the endothelial compartment facilitates proper vascular development and DV closure (Walisser et al. 2005). More recently, the *Ahr*^{fx} model has been used to show that the cell specific expression of AHR plays a critical role in maintaining homeostasis at barrier tissues like the lung, skin, and gut (Esser and Rannug 2015; Haas et al. 2016; Metidji et al. 2018). Use of the *Ahr*^{fx} models has been essential in

developing the hypothesis that AHR is an environmental and physiological sensor that monitors local chemistries to maintain homeostasis using a myriad of different mechanisms depending on cell type (Avilla et al. 2020; Esser and Rannug 2015; Quintana et al. 2008; Stockinger et al. 2014; Veldhoen et al. 2008).

While the *Ahr*^{fx} model has been an essential tool in the field of AHR biology, it is a conditional *Ahr*^{d} allele and thus has markedly reduced sensitivity to many classically defined ligands, as compared to *Ahr*^{b} strains (B6, C3H, BALB, etc.). The shortcoming of the *Ahr*^{fx} model is a consequence of the tools available at the time of its generation. That is, the allele was created by homologous recombination in 129SvJ-derived GS1 ESCs which harbor the low affinity *Ahr*^{d} allele (Poland et al. 1994; Walisser et al. 2005). Given that the low sensitivity of the *Ahr*^{fx} models can reduce statistical power and limit experimental protocols (Kennedy et al. 2014), we employed the ERA to target residue V375 in the *Ahr*^{fx} allele to create a model more sensitive to many xenobiotic ligands (Poland et al. 1994; Walisser et al. 2005). Residue 375 is a polymorphism located in the ligand binding pocket of AHR that is considered largely responsible for the differential ligand binding affinities between *Ahr*^{d} and *Ahr*^{b} alleles (Ema et al. 1994; Poland et al. 1994; Xing et al. 2012). In keeping with this idea, the conversion of *Ahr*^{fx} into *Ahr*^{V375A} improved the responsiveness to the xenobiotic AHR ligand βNF to levels comparable to those observed in B6 mice (Figure 4). While the conditional *Ahr*^{V375A} mice harbor other polymorphisms that exist between *Ahr*^{d} and *Ahr*^{b} alleles, including an alternate stop codon that yields an additional 43 amino acids on the C-terminus (Figure 3) (Poland et al. 1994). Our results suggest that these polymorphisms do not impact the AHR-driven gene induction following treatment with βNF (Figure 4).

The increased sensitivity and responsiveness of the *Ahr*^{V375A} mouse allows the use of nontoxic xenobiotic ligands like βNF, as well as short-term, acute exposure protocols. In comparison, prior experiments

employing the *Ahr*^{fx} allele required chronic exposures to highly potent and toxic ligands, such as TCDD, to induce a significant upregulation of target gene expression. An example of the type of information gained from use of the *Ahr*^{V375A} model can be seen with the deletion of the AHR in hepatocytes (*Ahr*^{V375A}*Cre*^{Alb}), where induction of *Cyp1a1* and *Cyp1a2* are almost completely abrogated, while induction of the *Cyp1b1* and *Ahrr* appear relatively unaffected following a four-hour exposure to 80 ug/kg βNF (Figure 7). This cell specific expression data is consistent with the idea that it is the AHR signaling in non-hepatocyte populations, e.g., Kuepfer cells, biliary epithelial cells, and/or endothelial cells, that is responsible for the upregulation of *Cyp1b1 and Ahrr* in liver. This observation was previously unobservable due to the insensitive nature of the *Ahr*^{fx} allele. Given the improved sensitivity of this model, it now seems possible to employ *Ahr*^{V375A} in future studies to examine the response of these gene targets in specific subpopulations. Importantly, use of *Ahr*^{V375A} supports the hypothesis that activation of the same cellular sensor, AHR, by the same ligand, βNF, is regulating different gene sets in different cell types within the same organ.

It is also important to note the unique genetics of *Ahr*^{V375A}. In addition to the conditional nature of the allele, it is also co-isogenic with the existing *Ahr*^{fx} model from which it was derived. All residues are identical between the two encoded proteins with the singular exception of residue 375. This co-isogenicity offers the first *in vivo* opportunity to examine the contribution of residue 375 in isolation on AHR-mediated endpoints in a conditional mouse model. While congenic lines like C57BL/6J-*Ahr*^{d} and DBA/2-*Ahr*^{b1} have proven valuable, those strains differ at residue 375, in addition to residues 324, 471, 532, and 588, and employ different stop codons (Poland et al. 1994). Importantly, the *Ahr*^{V375A} allele reported here is not identical to any known allele found in nature, but most closely resembles the *Ahr*^{b2} allele found in C3H and BALB/cBy mouse strains. That is, the *Ahr*^{V375A} allele harbors an A375, conferring

high affinity for ligand binding, and has the C-terminal extension of 43 amino acids common to *Ahr*^{b2} strains (in addition to the four other polymorphisms listed above).

It is known that CRISPR-Cas9 can yield unexpected mutations at or near the target site, often through the use of NHEJ rather than HDR to repair the induced double-stranded breaks (Sander and Joung 2014). In this case, we identified two such mutations and examined their consequences on AHR biology. The first of these mutations was the *Ahr*^{NG367R} mutant. Early characterization of this mutation presented as a null for the patent DV phenotype, liver lobe weights, and induction endpoints (Schmidt et al. 1996). Specifically, 100% of homozygous *Ahr*^{NG367R} and *Ahr* null mice exhibited a patent DV and were uninducible for target genes following ligand treatment (Table 2B, 3; Figure 5). This phenotypic evidence supports the hypothesis that *Ahr*^{NG367R} is a novel null allele. Protein analysis revealed that this protein is expressed, suggesting the null phenotype is not the consequence of a lack of protein, but rather a nonfunctional protein (Figure 3). Modelling of the AHR^{NG367R} protein suggests the mutation may significantly impact the tertiary structure of the PAS-B domain and could highlight the structural importance of the β hairpin in AHR structure (Figure 9). The mutation is located at the tip of the β hairpin, where G368 is missing and N367 is changed to R367. As a result, the RNGR sequence around the tip of the hairpin is converted to RRR. Glycine is energetically critical for the formation of the β-hairpin structure. In addition to the loss of the G368, this mutation creates a positive charged tip through the addition of Arginine, potentially disfavoring the formation of the β hairpin structure and resulting in significant changes in Hβ/Iβ, the two β sheets at the center of the "palm" of the ligand binding pocket (Xing et al. 2012). The structural alteration caused by this mutant may significantly affect the structure and stability of the ligand binding pocket and therefore impair ligand binding. This hypothesis is supported by the observation that homozygous mice harboring this mutation (*Ahr*$^{NG376R/NG367R}$) failed to respond to AHR ligand. While this mutation warrants further

characterization, this allele may have additional utility as a novel null allele that is co-isogenic with *Ahr*^{fx} and *Ahr*^{V375A}.

The other novel mutation that appears to have arisen through NHEJ is *Ahr*^{Ter383}. This allele encodes an adenine insertion at codon 371 resulting in a frameshift and premature stop codon at 383. Based upon previous domain mapping studies and structural models, we predicted this protein would behave as an antimorph and designed experiments to test this idea. In support of this prediction, we observed mice heterozygous for the wildtype *Ahr*^{b1} and *Ahr*^{Ter383} alleles (*Ahr*$^{b1/Ter383}$) display patent DV at a penetrance of 84%. This is compared to 0% patent DV in mice haploinsufficient for the *Ahr*^{b1} allele (*Ahr*$^{b1/-}$) (Table 2). This partial penetrance of DV has been observed in other AHR mutant mice, such as AHR and ARNT hypomorphs, as well as in mice haploinsufficient or hypomorphic for the AHR chaperone, Ara9 (Lin et al. 2008; Walisser et al. 2004a; Walisser et al. 2004b). Interestingly, while the *Ahr*^{Ter383} construct acts as a developmental antimorph (Table 2C, 3), it does not appear to affect induction of target genes like *Cyp1a1, Cyp1a2, Cyp1b1, and Ahrr* (Figure 6) or sensitivity to DSS-mediated colitis (Figure 8). The sequence of this mutant predicts the AHR^{Ter383} mutant has amino acid replacement beginning at residue 371 following the point mutation, altering the identity of the following eleven amino acids of the PAS-B domain (i.e., from YIIVTQRPLTD in *Ahr*^{fx} mice to IHHRHSETTDG-stop in *Ahr*^{Ter383} mice). This mutant protein retains the bHLH domain and the PAS-A domain, which together has been shown to confer full activity in ARNT dimerization (Seok et al. 2017). Thus, this mutant is postulated to retain the ability to dimerize with ARNT and interact with the target DNA sequences but may not be able to activate the transcription of downstream genes or respond to ligand given the missing C-terminal transactivation domain (Jain et al. 1994). Importantly, protein analysis reveals that AHR^{Ter383} produces a protein of predicted molecular weight around 42 kDa (Figure 3).

While there is still considerable work to be done to determine the mechanism by which *Ahr*^{Ter383} invokes its antimorphic activity during hepatovascular development, these observations suggest the developmental pathway has different requirements for AHR and ARNT concentrations than the adaptive pathway or other physiological pathways such as that employed in intestinal barrier integrity. While such ideas can be investigated in future studies, it is important to note that the *Ahr*^{Ter383} allele may have significant utility in AHR mechanism of action studies *in vivo*. It is not only antimorphic for the DV endpoint, but this activity is conditional, as the allele can be excised by cell specific *Cre* recombinase (Table 5). When crossed to a mouse harboring the endothelial specific *Cre*^{Cdh5} transgene, normal DV closure proceeds, demonstrating that removal of *Ahr*^{T383} in endothelial cells rescues the DV phenotype. This is consistent with the observation that mice conditional for *Ahr*^{fx} crossed to mice harboring the *Cre*^{Cdh5} transgene (*Ahr*$^{fx/fx}$*Cre*^{Cdh5}) exhibit a patent DV (Walisser et al. 2005).

The *Ahr*^{V375A} mouse was generated intentionally to solve the problem of xenobiotic sensitivity in the existing conditional model and serve as a useful tool in future cell autonomy, toxicology, drug metabolism, and immunology studies. Though generated serendipitously, the two other novel mutations described may also be useful in AHR biology studies. The *Ahr*^{NG367R} mouse is a potentially novel null allele that is co-isogenic with the other models in this series and provides a useful model in AHR protein structure studies. The *Ahr*^{Ter383} mouse model could prove useful in studies of patent DV due to the fact that the model may be used as a heterozygote, which helps to cut time and breeding requirements for experiments. Additionally, this allele may be optimized to generate an even more effective AHR antimorph and serve as a model for creating antimorphs in other PAS proteins. These studies remain on going, but our early characterization has shown that these animals may be useful to other laboratories working to better understand AHR biology.

ACKNOWLEDGEMENTS

This work was supported by the National Institutes of Health Grants R35-ES028377, T32-ES007015, T32-GM008692, T32-CA009135, and P30-CA014520. The UW SciMed GRS Program and The Morgridge Foundation. Thank you to Katie Stanley of the Arts and Media Solutions division at the University of Wisconsin-Madison School of Medicine and Public Health for contributing to figure design and digitalization.

REFERENCES

Adli M. 2018. The crispr tool kit for genome editing and beyond. Nature Communications. 9(1):1911.

Alva JA, Zovein AC, Monvoisin A, Murphy T, Salazar A, Harvey NL, Carmeliet P, Iruela-Arispe ML. 2006. Ve-cadherin-cre-recombinase transgenic mouse: A tool for lineage analysis and gene deletion in endothelial cells. Dev Dyn. 235(3):759-767.

Aryal NK, Wasylishen AR, Lozano G. 2018. Crispr/cas9 can mediate high-efficiency off-target mutations in mice in vivo. Cell Death & Disease. 9(11):1099.

Avilla MN, Malecki KMC, Hahn ME, Wilson RH, Bradfield CA. 2020. The ah receptor: Adaptive metabolism, ligand diversity, and the xenokine model. Chem Res Toxicol. 33(4):860-879.

Baker BB, Yee JS, Meyer DN, Yang D, Baker TR. 2016. Histological and transcriptomic changes in male zebrafish testes due to early life exposure to low level 2,3,7,8-tetrachlorodibenzo-p-dioxin. Zebrafish. 13(5):413-423.

Baricza E, Tamasi V, Marton N, Buzas EI, Nagy G. 2016. The emerging role of aryl hydrocarbon receptor in the activation and differentiation of th17 cells. Cellular and Molecular Life Sciences. 73(1):95-117.

Bhaumik S, Basu R. 2017. Cellular and molecular dynamics of th17 differentiation and its developmental plasticity in the intestinal immune response. Frontiers in Immunology. 8:20.

Bunger MK, Glover E, Moran SM, Walisser JA, Lahvis GP, Hsu EL, Bradfield CA. 2008. Abnormal liver development and resistance to 2,3,7,8-tetrachlorodibenzo-p-dioxin toxicity in mice carrying a mutation in the dna-binding domain of the aryl hydrocarbon receptor. Toxicol Sci. 106(1):83-92.

Bunger MK, Moran SM, Glover E, Thomae TL, Lahvis GP, Lin BC, Bradfield CA. 2003. Resistance to 2,3,7,8-tetrachlorodibenzo-p-dioxin toxicity and abnormal liver development in mice carrying a mutation in the nuclear localization sequence of the aryl hydrocarbon receptor. J Biol Chem. 278(20):17767-17774.

Ceccaldi R, Rondinelli B, D'Andrea AD. 2016. Repair pathway choices and consequences at the double-strand break. Trends Cell Biol. 26(1):52-64.

Cella M, Colonna M. 2015. Aryl hydrocarbon receptor: Linking environment to immunity. Seminars in Immunology. 27(5):310-314.

Dragin N, Shi Z, Madan R, Karp CL, Sartor MA, Chen C, Gonzalez FJ, Nebert DW. 2008. Phenotype of the cyp1a1/1a2/1b1-/- triple-knockout mouse. Mol Pharmacol. 73(6):1844-1856.

Díaz-Díaz CJ, Ronnekleiv-Kelly SM, Nukaya M, Geiger PG, Balbo S, Dator R, Megna BW, Carney PR, Bradfield CA, Kennedy GD. 2016. The aryl hydrocarbon receptor is a repressor of inflammation-associated colorectal tumorigenesis in mouse. Ann Surg. 264(3):429-436.

Ema M, Ohe N, Suzuki M, Mimura J, Sogawa K, Ikawa S, Fujii-Kuriyama Y. 1994. Dioxin binding activities of polymorphic forms of mouse and human arylhydrocarbon receptors. Journal of Biological Chemistry. 269(44):27337-27343.

Esser C. 2016. The aryl hydrocarbon receptor in immunity: Tools and potential. Methods Mol Biol. 1371:239-257.

Esser C, Rannug A. 2015. The aryl hydrocarbon receptor in barrier organ physiology, immunology, and toxicology. Pharmacological Reviews. 67(2):259.

Furumatsu K, Nishiumi S, Kawano Y, Ooi M, Yoshie T, Shiomi Y, Kutsumi H, Ashida H, Fujii-Kuriyama Y, Azuma T et al. 2011. A role of the aryl hydrocarbon receptor in attenuation of colitis. Digestive Diseases and Sciences. 56(9):2532-2544.

Haas K, Weighardt H, Deenen R, Köhrer K, Clausen B, Zahner S, Boukamp P, Bloch W, Krutmann J, Esser C. 2016. Aryl hydrocarbon receptor in keratinocytes is essential for murine skin barrier integrity. Journal of Investigative Dermatology. 136(11):2260-2269.

Hahn ME. 2002. Aryl hydrocarbon receptors: Diversity and evolution. Chem Biol Interact. 141(1-2):131-160.

Harrill JA, Hukkanen RR, Lawson M, Martin G, Gilger B, Soldatow V, Lecluyse EL, Budinsky RA, Rowlands JC, Thomas RS. 2013. Knockout of the aryl hydrocarbon receptor results in distinct hepatic and renal phenotypes in rats and mice. Toxicol Appl Pharmacol. 272(2):503-518.
Harstad EB, Guite CA, Thomae TL, Bradfield CA. 2006. Liver deformation in ahr-null mice: Evidence for aberrant hepatic perfusion in early development. Mol Pharmacol. 69(5):1534-1541.
Jain S, Dolwick KM, Schmidt JV, Bradfield CA. 1994. Potent transactivation domains of the ah receptor and the ah receptor nuclear translocator map to their carboxyl termini. J Biol Chem. 269(50):31518-31524.
Kennedy GD, Nukaya M, Moran SM, Glover E, Weinberg S, Balbo S, Hecht SS, Pitot HC, Drinkwater NR, Bradfield CA. 2014. Liver tumor promotion by 2,3,7,8-tetrachlorodibenzo-p-dioxin is dependent on the aryl hydrocarbon receptor and tnf/il-1 receptors. Toxicol Sci. 140(1):135-143.
Kiss EA, Vonarbourg C, Kopfmann S, Hobeika E, Finke D, Esser C, Diefenbach A. 2011. Natural aryl hydrocarbon receptor ligands control organogenesis of intestinal lymphoid follicles. Science. 334(6062):1561-1565.
Lahvis GP, Lindell SL, Thomas RS, McCuskey RS, Murphy C, Glover E, Bentz M, Southard J, Bradfield CA. 2000. Portosystemic shunting and persistent fetal vascular structures in aryl hydrocarbon receptor-deficient mice. Proc Natl Acad Sci U S A. 97(19):10442-10447.
Lahvis GP, Pyzalski RW, Glover E, Pitot HC, McElwee MK, Bradfield CA. 2005. The aryl hydrocarbon receptor is required for developmental closure of the ductus venosus in the neonatal mouse. Mol Pharmacol. 67(3):714-720.
LaPres JJ, Glover E, Dunham EE, Bunger MK, Bradfield CA. 2000. Ara9 modifies agonist signaling through an increase in cytosolic aryl hydrocarbon receptor. J Biol Chem. 275(9):6153-6159.
Larigot L, Juricek L, Dairou J, Coumoul X. 2018. Ahr signaling pathways and regulatory functions. Biochimie Open. 7:1-9.
Lin BC, Nguyen LP, Walisser JA, Bradfield CA. 2008. A hypomorphic allele of aryl hydrocarbon receptor-associated protein-9 produces a phenocopy of the ahr-null mouse. Mol Pharmacol. 74(5):1367-1371.
Mali P, Yang L, Esvelt KM, Aach J, Guell M, DiCarlo JE, Norville JE, Church GM. 2013. Rna-guided human genome engineering via cas9. Science. 339(6121):823-826.
McIntosh BE, Hogenesch JB, Bradfield CA. 2010. Mammalian per-arnt-sim proteins in environmental adaptation. Annu Rev Physiol. 72:625-645.
Metidji A, Omenetti S, Crotta S, Li Y, Nye E, Ross E, Li V, Maradana MR, Schiering C, Stockinger B. 2018. The environmental sensor ahr protects from inflammatory damage by maintaining intestinal stem cell homeostasis and barrier integrity. Immunity. 49(2):353-362.
Nebert DW. 2017. Aryl hydrocarbon receptor (ahr): "Pioneer member" Of the basic-helix/loop/helix per-arnt-sim (bhlh/pas) family of "Sensors" Of foreign and endogenous signals. Progress in lipid research. 67:38-57.
Nebert DW, Gelboin HV. 1969. The in vivo and in vitro induction of aryl hydrocarbon hydroxylase in mammalian cells of different species, tissues, strains, and developmental and hormonal states. Arch Biochem Biophys. 134(1):76-89.
Nebert DW, Robinson JR, Niwa A, Kumari K, Poland AP. 1975. Genetic expression of aryl hydrocarbon hydroxylase activity in the mouse. Journal of Cellular Physiology. 85(S1):393-414.
Poland A, Glover E. 1975. Genetic expression of aryl hydrocarbon hydroxylase by 2,3,7,8-tetrachlorodibenzo-p-dioxin: Evidence for a receptor mutation in genetically non-responsive mice. Molecular Pharmacology. 11(4):389-398.
Poland A, Glover E. 1980. 2,3,7,8,-tetrachlorodibenzo-p-dioxin: Segregation of toxocity with the ah locus. Mol Pharmacol. 17(1):86-94.

Poland A, Glover E. 1990. Characterization and strain distribution pattern of the murine ah receptor specified by the ahd and ahb-3 alleles. Mol Pharmacol. 38(3):306-312.
Poland A, Glover E, Bradfield CA. 1991. Characterization of polyclonal antibodies to the ah receptor prepared by immunization with a synthetic peptide hapten. Mol Pharmacol. 39(1):20-26.
Poland A, Glover E, Kende AS. 1976. Stereospecific, high affinity binding of 2,3,7,8-tetrachlorodibenzo-p-dioxin by hepatic cytosol. Evidence that the binding species is receptor for induction of aryl hydrocarbon hydroxylase. J Biol Chem. 251(16):4936-4946.
Poland A, Palen D, Glover E. 1994. Analysis of the four alleles of the murine aryl hydrocarbon receptor. Mol Pharmacol. 46(5):915-921.
Pollenz RS, Sattler CA, Poland A. 1994. The aryl hydrocarbon receptor and aryl hydrocarbon receptor nuclear translocator protein show distinct subcellular localizations in hepa 1c1c7 cells by immunofluorescence microscopy. Molecular Pharmacology. 45(3):428.
Postic C, Shiota M, Niswender KD, Jetton TL, Chen Y, Moates JM, Shelton KD, Lindner J, Cherrington AD, Magnuson MA. 1999. Dual roles for glucokinase in glucose homeostasis as determined by liver and pancreatic beta cell-specific gene knock-outs using cre recombinase. J Biol Chem. 274(1):305-315.
Quintana FJ, Basso AS, Iglesias AH, Korn T, Farez MF, Bettelli E, Caccamo M, Oukka M, Weiner HL. 2008. Control of t(reg) and t(h)17 cell differentiation by the aryl hydrocarbon receptor. Nature. 453(7191):65-71.
Ran FA, Hsu PD, Wright J, Agarwala V, Scott DA, Zhang F. 2013. Genome engineering using the crispr-cas9 system. Nat Protoc. 8(11):2281-2308.
Sander JD, Joung JK. 2014. Crispr-cas systems for editing, regulating and targeting genomes. Nature Biotechnology. 32(4):347-355.
Schmidt JV, Su GH, Reddy JK, Simon MC, Bradfield CA. 1996. Characterization of a murine ahr null allele: Involvement of the ah receptor in hepatic growth and development. Proc Natl Acad Sci U S A. 93(13):6731-6736.
Seok SH, Lee W, Jiang L, Molugu K, Zheng A, Li Y, Park S, Bradfield CA, Xing Y. 2017. Structural hierarchy controlling dimerization and target dna recognition in the ahr transcriptional complex. Proc Natl Acad Sci U S A.
Singh P, Schimenti JC, Bolcun-Filas E. 2015. A mouse geneticist's practical guide to crispr applications. Genetics. 199(1):1-15.
Stevens EA, Mezrich JD, Bradfield CA. 2009. The aryl hydrocarbon receptor: A perspective on potential roles in the immune system. Immunology. 127(3):299-311.
Stockinger B, Meglio PD, Gialitakis M, Duarte JH. 2014. The aryl hydrocarbon receptor: Multitasking in the immune system. Annual Review of Immunology. 32(1):403-432.
Veldhoen M, Hirota K, Westendorf AM, Buer J, Dumoutier L, Renauld J-C, Stockinger B. 2008. The aryl hydrocarbon receptor links th17-cell-mediated autoimmunity to environmental toxins. Nature. 453(7191):106-109.
Villa M, Gialitakis M, Tolaini M, Ahlfors H, Henderson CJ, Wolf CR, Brink R, Stockinger B. 2017. Aryl hydrocarbon receptor is required for optimal b-cell proliferation. The EMBO Journal. 36(1):116-128.
Walisser JA, Bunger MK, Glover E, Bradfield CA. 2004a. Gestational exposure of ahr and arnt hypomorphs to dioxin rescues vascular development. Proc Natl Acad Sci U S A. 101(47):16677-16682.
Walisser JA, Bunger MK, Glover E, Harstad EB, Bradfield CA. 2004b. Patent ductus venosus and dioxin resistance in mice harboring a hypomorphic arnt allele. J Biol Chem. 279(16):16326-16331.

Walisser JA, Glover E, Pande K, Liss AL, Bradfield CA. 2005. Aryl hydrocarbon receptor-dependent liver development and hepatotoxicity are mediated by different cell types. Proceedings of the National Academy of Sciences. 102(49):17858-17863.

Xing Y, Nukaya M, Satyshur KA, Jiang L, Stanevich V, Korkmaz EN, Burdette L, Kennedy GD, Cui Q, Bradfield CA. 2012. Identification of the ah-receptor structural determinants for ligand preferences. Toxicol Sci. 129(1):86-97.

Table 1. Nomenclature for *Ahr* alleles.

Mouse strain	Formal name	Informal name	Technology	Description
Wildtype	C57BL/6J	Ahr^{b1}	n/a	Wildtype allele found in B6 mice
Conditional	$Ahr^{tm3.1Bra}$	Ahr^{fx}	Homologous Recombination	Low affinity conditional allele; generated from 129Sv ESCs (Ahr^{d} at the *Ahr* locus)
Null	$Ahr^{.1Bra}$	$Ahr^{-/-}$	Homologous Recombination	Exon 2 removed; generated from 129Sv ESCs cells (Ahr^{d} at the *Ahr* locus)
High affinity conditional	Ahr^{em1Bra}	Ahr^{V375A}	CRISPR-Cas9	High affinity conditional allele; Ahr^{d} at the *Ahr* locus except for a single nucleotide polymorphism at residue 375 introduced via homology directed repair
Ahr^{NG367R}	Ahr^{em2Bra}	Ahr^{NG367R}	CRISPR-Cas9	Three base pair deletion near ligand binding domain generated through nonhomologous end joining; conditional; Ahr^{d} at the *Ahr* locus
Ahr^{Ter383}	Ahr^{em3Bra}	Ahr^{Ter383}	CRISPR-Cas9	Single nucleotide insertion generated through nonhomologous end joining; fame shift at residue 371 results in 11 amino acid changes and early termination at 383; conditional

Mouse common name refers to the name commonly used in manuscripts and scientific presentations. Includes the formal locus names defined by the International Committee on Standardized Genetic Nomenclature for Mice and assigned by Jackson Laboratory. The informal locus names of alleles used in this paper are defined. The technology column described the technique used to generate each model, followed by a brief description of important allelic traits.

Table 2. Patent DV frequencies in the three alleles.

A. *V375A*

Genotype	% patent DV	n
$Ahr^{b1/b1}$	0	0/8
$Ahr^{fx/fx}$	0	0/12
$Ahr^{b1/V375A}$	0	0/9
$Ahr^{V375A/V375A}$	0	0/10

B. *NG367R*

Genotype	% patent DV	n
$Ahr^{b1/b1}$	0	0/6
$Ahr^{b1/NG367R}$	0	0/11
$Ahr^{NG367R/NG367R}$	100	13/13
$Ahr^{-/-}$	100	15/15

C. *Ter383*

Genotype	% patent DV	n
$Ahr^{b1/b1}$	0	0/10
$Ahr^{b1/-}$	0	0/13
$Ahr^{-/-}$	100	15/15
$Ahr^{b1/Ter383}$	84	16/19
$Ahr^{Ter383/Ter383}$	100	9/9

A. Penetrance of patent DV in Ahr^{V375A} mutants and relevant controls. B. Penetrance of DV in ligand binding Ahr^{NG367R} mutants and controls. C. Penetrance of DV in truncated Ahr^{Ter383} mutants and appropriate controls. The DV penetrance is measured by portal vein gravity flow perfusion. Roughly equal numbers of male and female mice are represented within each genotype. Statistical analysis using a Chia squared (Fisher's exact test) shows no significant differences between $Ahr^{V375A/V375A}$ and controls ($Ahr^{b1/b1}$, $Ahr^{fx/fx}$, and $Ahr^{b1/V375A}$); significant differences between $Ahr^{NG367R/NG367R}$ and $Ahr^{-/-}$ versus wildtype controls ($Ahr^{b1/b1}$ and $Ahr^{b1/NG367R}$)($p < 0.0001$); and a statistical difference between $Ahr^{b1/Ter38}$, $Ahr^{Ter383/Ter383}$, and $Ahr^{-/-}$ versus wildtype and haploinsufficient controls ($Ahr^{b1/b1}$ and $Ahr^{b1/-}$)($p < 0.0001$).

Table 3. Liver lobe weights in the three mutants.

Genotype	Left: median lobe weight (mean ± SD)	n
Ahr$^{b1/b1}$	1.14 ± 0.13	19
Ahr$^{fx/fx}$	1.06 ± 0.13	6
Ahr$^{-/-}$	0.75 ± 0.04	6
Ahr$^{V375A/V365A}$	1.14 ± 0.12	9
Ahr$^{NG367R/NG367R}$	0.92 ± 0.14	10
Ahr$^{b1/Ter383}$	0.84 ± 0.18	12

Left: median liver lobe weight ratios from homozygous *Ahr*$^{V375A/V375A}$ and *Ahr*$^{NG367R/NG367R}$ mice, as well as heterozygous *Ahr*$^{b1/Ter383}$ mice relative to *Ahr*$^{b1/b1}$, *Ahr*$^{fx/fx}$, and *Ahr*$^{-/-}$ controls. Rations of all the mice within a given genotype are represented as the mean weights of left to median lobes ± standard deviation. Roughly equal numbers of male and female mice are represented for each genotype. Statistical analysis using a one-way ANOVA shows significant differences between the livers of *Ahr*$^{b1/b1}$, *Ahr*$^{fx/fx}$, and *Ahr*$^{b1/V375A}$ mice compared to *Ahr*$^{-/-}$, *Ahr*$^{NG367R/NG367R}$ and *Ahr*$^{b1/Ter383}$ mice ($p < 0.0001$).

Table 4. Penetrance of DV in V375A mutants crossed to mice harboring hepatocyte (*Alb*) and endothelial (*Cdh5*) driven *Cre* recombinase.

Ahr genotype	*Cre*	% patent DV	n
Ahr$^{V375A/V375A}$	(none)	0	0/15
Ahr$^{V375A/V375A}$	*Alb*	0	0/10
Ahr$^{V375A/V375A}$	*Cdh5*	100	10/10

Excision of the *Ahr*^{V375A} allele in hepatocytes does not result in patent DV in (*Ahr*^{V375A}*Cre*^{Alb}) animals. Excision of the *Ahr*^{V375A} allele in endothelial cells results in patent DV in (*Ahr*^{V375A}*Cre*^{Cdh5}) animals. Roughly equal numbers of male and female mice are represented for each genotype. Statistical analysis using a Chia squared (Fisher's exact test) shows significant differences between *Ahr*^{V375A} and *Ahr*^{V375A}*Cre*^{Alb} versus *Ahr*^{V375A}*Cre*^{Cdh5}($p < 0.0001$). There is no signficant dfference between *Ahr*$^{V375A/V375A}$ and *Ahr*$^{V375A/V375A}$*Cre*^{Alb}.

Table 5. Penetrance of DV in truncated *Ter383* mutants crossed to endothelial specific (*Cre^{Cdh5}*) Cre recombinase.

Ahr genotype	*Cre^{Cdh5}* genotype	% patent DV	n
Ahr$^{b1/b1}$	-	0	0/10
Ahr$^{b1/b1}$	+	0	0/10
Ahr$^{b1/Ter383}$	-	86	19/22
Ahr$^{b1/Ter383}$	+	19	2/11

Excision of the *Ahr^{Ter383}* allele rescues DV closure in heterozygous (*Ahr$^{b1/Ter383}$ Cre^{Cdh5}*) animals. Roughly equal numbers of male and female mice are represented for each genotype. Statistical analysis using a Chia squared (Fisher's exact test) shows significant differences between *Ahr$^{b1/Ter383}$* versus *Ahr$^{b1/Ter383}$ Cre^{Cdh5}* ($p = 0.0002$). There is no signficant dfference between *Ahr$^{b1/1b1}$*, *Ahr$^{b1/b1}$Cre^{Cdh51}*, and *Ahr$^{b1/Ter383}$ Cre^{Cdh5}*.

Figure Legends

Figure 1. Gene editing strategy for CRISPR-generated mutant mice. Allels are shown in chronological order for which they were generated. The *Ahr*^{NG367R} allele was generated in an independent experiment, whereas *Ahr*^{V375A} and *Ahr*^{Ter383} alleles were generated on separate chromosomes in the same mouse during a separate experiment. A. Proposed mechanism generating *Ahr*^{NG367R} allele. The Cas9 endonuclease incorporates guide RNA #1, directing the Cas9 protein to the *Ahr* locus in *Ahr*^{fx} embryos. The Cas9 cleaves the DNA at the PAM sequence, inducing a double stranded break. The cell recognizes the double stranded break and repairs the break using nonhomologous end joining. In this case, three base pairs are deleted resulting in the *Ahr*^{NG367R} mutation. B. Proposed mechanism generating the *Ahr*^{V375A} and *Ahr*^{Ter383} alleles. Guide RNA #2 directs Cas9 endonuclease in *Ahr*^{fx} embryos. The Cas9 cleaves the DNA at the PAM site, inducing a double stranded break. On one chromosome (left), the break is repaired through nonhomologous end joining, resulting in a single nucleotide insertion at the *Ahr* locus and the *Ahr*^{Ter383} mutation. On the second chromosome (right), the cell recognizes homology with the ssODN. Homology directed repair guides incorporation of the soodn sequence into the genome at the *Ahr* locus, resulting in incorporation of the *Ahr*^{V375A} mutation. Both mutations occurred in one mouse, but each mutation occurred on a separate chromosome. The lines were separated into distinct lines through breeding with wildtype B6 mice.

Figure 2. Gene structure and protein map of induced mutations. Green boxes represent exons corresponding to amino acids in the bHLH domain, blue boxes represent the PAS domain, and yellow represents the transactivation domain. Red arrows represent *loxP* sites flanking exon-2. Boxes above each allele show the DNA sequence; boxes below each allele describe amino acids. A. Protein map for the *V375A* allele. The gene encodes for a point mutation at residue 375, changing GTC (Valine) to GCC (Alanine). B. Protein map for the *NG367R* allele. At the *Ahr* locus, three base pairs [ATG] are deleted in the genome, resulting in an amino acid substitution (NG367R) and a mutated PAS-B and ligand binding domain. The deleted nucleotides are designated by brackets in the DNA sequence. C. Protein map for the *Ter383* allele based on genomic mutations. There is an adenine insertion at the codon for residue 371 in the gene results in a frame shift and early termination at residue 383. The dark blue represents amino acids following 371 that have been altered as a result of the frame shift.

Figure 3. Expression of mutant proteins. A. The epitope for the BEAR-3 antibody recognizes amino acids 1-402 of AHR^{b1}. The protein products from the recombinant four *Ahr* alleles are shown relative to AHR^{b1}. The asterisk (*) denotes SNPs in AHR^{fx} relative to AHR^{b1}. The # denoted the V375A mutation in AHR^{V375A}. The ^ marks the NG367R mutation in AHR^{NG367R} resulting from a three base pair deletion spanning codons 367 and 368, yielding a single amino acid deletion and a change in residue 367. Expected protein size is shown next to each predicted protein map. B. Western Blot shows 63 ug of protein products using BEAR-3 antibody. Cytosols were isolated fresh from two adult mice homozygous for each genotype. Image is representative of two experiments.

Figure 4. Induction of AHR-driven genes in high affinity conditional mutants (*Ahr*^{V375A}). Induction of AHR-driven genes in homozygous high affinity conditional mutant (*Ahr*^{V375A}) compared to mice homozygous for the low affinity conditional allele (*Ahr*^{fx}) and homozygous wildtype animals (*Ahr*^{b1}). Mice are treated with βNF or corn oil vehicle control (CO) for four hours. Liver mRNA expression of AHR-driven genes relative to *Hprt.* Groups sharing a superscript are not different at the level of statistical

significance ($p > 0.05$). Each point represents the mean of three technical replicates of one biological replicate. Males are represented by a circle while females are represented by a square. Error bars represent standard error of the mean.

Figure 5. Induction of AHR-driven genes in the 3 base pair deletion mutant (*Ahr^{NG367R}*). Induction of AHR-driven genes in homozygous ligand binding mutant (*Ahr^{NG367R}*) compared to mice homozygous for the high affinity conditional allele (*Ahr^{V375A}*). Mice are treated with βNF or corn oil vehicle control (CO) for four hours. Liver mRNA expression of AHR-driven genes relative to *Hprt.* Groups sharing a superscript are not different at the level of statistical significance ($p > 0.05$). Each point represents the mean of three technical replicates of one biological replicate. Males are represented by a circle while females are represented by a square. Error bars represent standard error of the mean.

Figure 6. Induction of AHR-driven genes in heterozygous truncated mutants (*Ahr$^{b1/Ter383}$*). Induction of AHR-driven genes in heterozygous truncated mutants (*Ahr$^{b1/Ter383}$*) compared to homozygous wildtype (*Ahr$^{b1/b1}$*) and haploinsufficient (*Ahr$^{b1/-}$*) controls. Mice are treated with βNF or corn oil vehicle control (CO) for four hours. Liver mRNA expression of AHR-driven genes relative to *Hprt.* Groups sharing a superscript are not different at the level of statistical significance ($p > 0.05$). Each point represents the mean of three technical replicates of one biological replicate. Males are represented by a circle while females are represented by a square. Error bars represent standard error of the mean.

Figure 7. Induction of AHR-driven genes in the high affinity conditional allele excised in hepatocytes (*Ahr^{V375A}Cre^{Alb}*). Induction of AHR-driven genes in mice ubiquitously expressing the high affinity conditional allele (*Ahr^{GN367R}*) compared to mice with the AHR excised in hepatocytes (*Ahr^{V375A}Cre^{Alb}*). Mice are treated with βNF or corn oil vehicle control (CO) for four hours. Liver mRNA expression of AHR-driven genes relative to *Hprt.* Groups sharing a superscript are not different at the level of statistical significance ($p > 0.05$). Each point represents the mean of three technical replicates of one biological replicate. Males are represented by a circle while females are represented by a square. Error bars represent standard error of the mean.

Figure 8. Colitis phenotype in *Ahr$^{b1/Ter383}$* mice. A. Colon length of mice treated with 1% DSS in drinking water for 5 days. Differences between groups sharing a superscript are not statistically significant. B. Relative expression of *Il1b* and *Rorc* mRNA transcripts in whole colon of mice treated with 1% DSS in drinking water for 5 days. Differences between groups sharing a superscript are not statistically significant. Roughly equal numbers of males and females are represented in each genotype. Each point represents the mean of three technical replicates of one biological replicate. Error bars represent standard error of the mean.

Figure 9. Structural rendition of PAS-B from AHR^{b1} showing location of amino acids relevant to mutants. The structure of the PAS-B domain modeled from AHR^{b1} sequence is shown in light blue. A TCDD molecule is shown in the ligand binding pocket in yellow. Residue 375 (Alanine) is highlighted in purple. The Glycine residue at 368 mutated in the AHR^{NG367R} model is highlighted in red, located in the hairpin loop. The residues changed in AHR^{Ter383} are highlighted in dark blue.

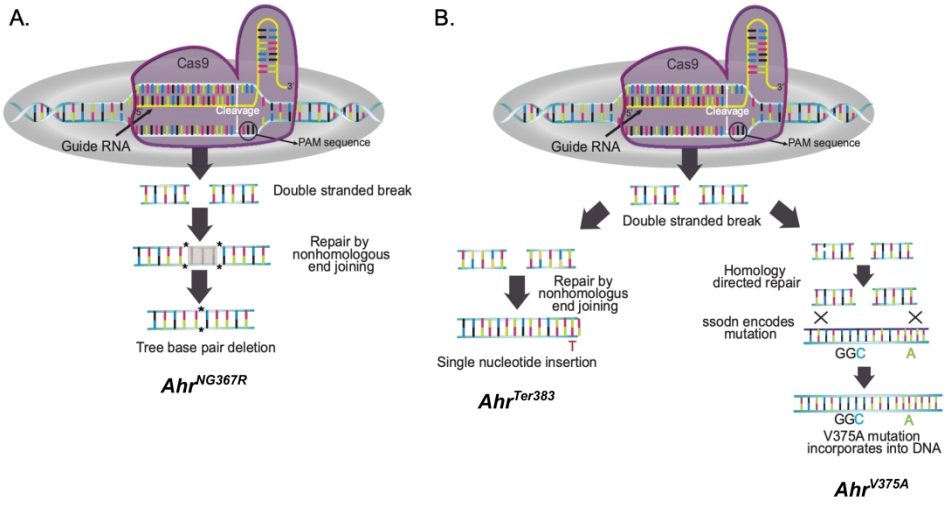

Figure 1. Gene editing strategy for CRISPR-generated mutant mice. Allels are shown in chronological order for which they were generated. The AhrNG367R allele was generated in an independent experiment, whereas AhrV375A and AhrTer383 alleles were generated on separate chromosomes in the same mouse during a separate experiment. A. Proposed mechanism generating AhrNG367R allele. The Cas9 endonuclease incorporates guide RNA #1, directing the Cas9 protein to the Ahr locus in Ahrfx embryos. The Cas9 cleaves the DNA at the PAM sequence, inducing a double stranded break. The cell recognizes the double stranded break and repairs the break using nonhomologous end joining. In this case, three base pairs are deleted resulting in the AhrNG367R mutation. B. Proposed mechanism generating the AhrV375A and AhrTer383 alleles. Guide RNA #2 directs Cas9 endonuclease in Ahrfx embryos. The Cas9 cleaves the DNA at the PAM site, inducing a double stranded break. On one chromosome (left), the break is repaired through nonhomologous end joining, resulting in a single nucleotide insertion at the Ahr locus and the AhrTer383 mutation. On the second chromosome (right), the cell recognizes homology with the ssODN. Homology directed repair guides incorporation of the soodn sequence into the genome at the Ahr locus, resulting in incorporation of the AhrV375A mutation. Both mutations occurred in one mouse, but each mutation occurred on a separate chromosome. The lines were separated into distinct lines through breeding with wildtype B6 mice.

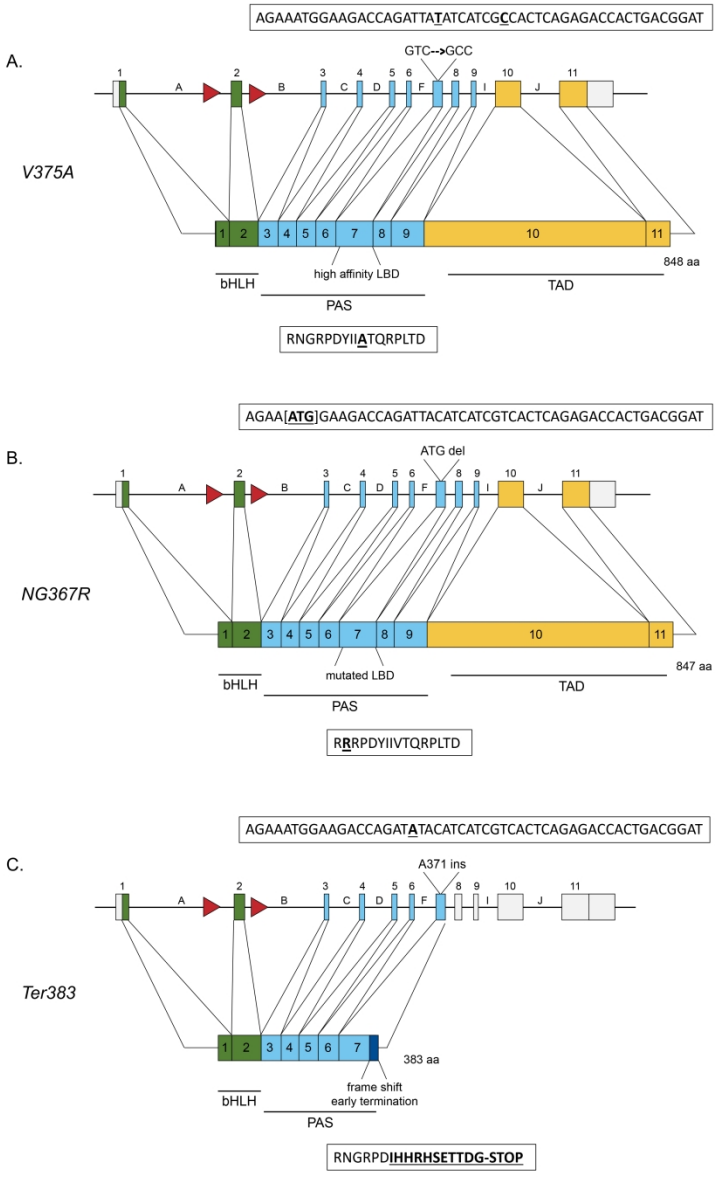

Figure 2. Gene structure and protein map of induced mutations. Green boxes represent exons corresponding to amino acids in the bHLH domain, blue boxes represent the PAS domain, and yellow represents the transactivation domain. Red arrows represent IoxP sites flanking exon-2. Boxes above each allele show the DNA sequence; boxes below each allele describe amino acids. A. Protein map for the V375A allele. The gene encodes for a point mutation at residue 375, changing GTC (Valine) to GCC (Alanine). B. Protein map for the NG367R allele. At the Ahr locus, three base pairs [ATG] are deleted in the genome, resulting in an amino acid substitution (NG367R) and a mutated PAS-B and ligand binding domain. The deleted nucleotides are designated by brackets in the DNA sequence. C. Protein map for the Ter383 allele based on genomic mutations. There is an adenine insertion at the codon for residue 371 in the gene results in a frame shift and early termination at residue 383. The dark blue represents amino acids following 371 that have been altered as a result of the frame shift.

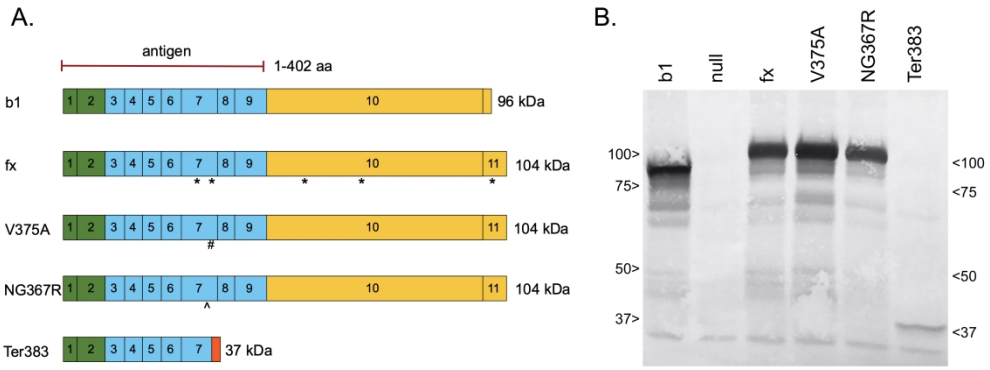

Figure 3. Expression of mutant proteins. A. The epitope for the BEAR-3 antibody recognizes amino acids 1-402 of AHRb1. The protein products from the recombinant four Ahr alleles are shown relative to AHRb1. The asterisk (*) denotes SNPs in AHRfx relative to AHRb1. The # denoted the V375A mutation in AHRV375A. The ^ marks the NG367R mutation in AHRNG367R resulting from a three base pair deletion spanning codons 367 and 368, yielding a single amino acid deletion and a change in residue 367. Expected protein size is shown next to each predicted protein map. B. Western Blot shows 63 ug of protein products using BEAR-3 antibody. Cytosols were isolated fresh from two adult mice homozygous for each genotype. Image is representative of two experiments.

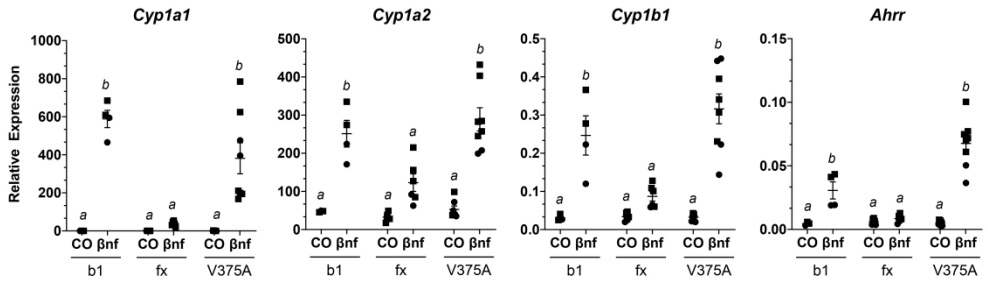

Figure 4. Induction of AHR-driven genes in high affinity conditional mutants (AhrV375A). Induction of AHR-driven genes in homozygous high affinity conditional mutant (AhrV375A) compared to mice homozygous for the low affinity conditional allele (Ahrfx) and homozygous wildtype animals (Ahrb1). Mice are treated with βNF or corn oil vehicle control (CO) for four hours. Liver mRNA expression of AHR-driven genes relative to Hprt. Groups sharing a superscript are not different at the level of statistical significance ($p > 0.05$). Each point represents the mean of three technical replicates of one biological replicate. Males are represented by a circle while females are represented by a square.

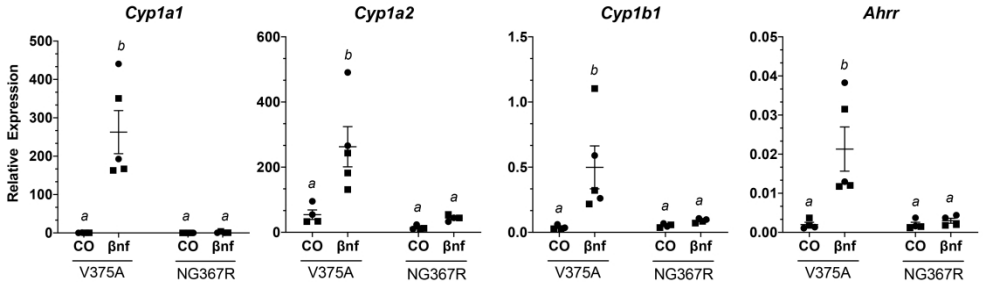

Figure 5. Induction of AHR-driven genes in the 3 base pair deletion mutant (AhrNG367R). Induction of AHR-driven genes in homozygous ligand binding mutant (AhrNG367R) compared to mice homozygous for the high affinity conditional allele (AhrV375A). Mice are treated with βNF or corn oil vehicle control (CO) for four hours. Liver mRNA expression of AHR-driven genes relative to Hprt. Groups sharing a superscript are not different at the level of statistical significance ($p > 0.05$). Each point represents the mean of three technical replicates of one biological replicate. Males are represented by a circle while females are represented by a square.

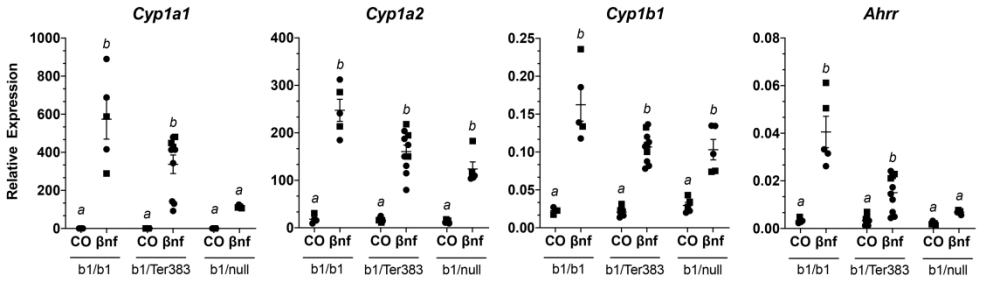

Figure 6. Induction of AHR-driven genes in heterozygous truncated mutants (Ahrb1/Ter383). Induction of AHR-driven genes in heterozygous truncated mutants (Ahrb1/Ter383) compared to homozygous wildtype (Ahrb1/b1) and haploinsufficient (Ahrb1/-) controls. Mice are treated with βNF or corn oil vehicle control (CO) for four hours. Liver mRNA expression of AHR-driven genes relative to Hprt. Groups sharing a superscript are not different at the level of statistical significance ($p > 0.05$). Each point represents the mean of three technical replicates of one biological replicate. Males are represented by a circle while females are represented by a square.

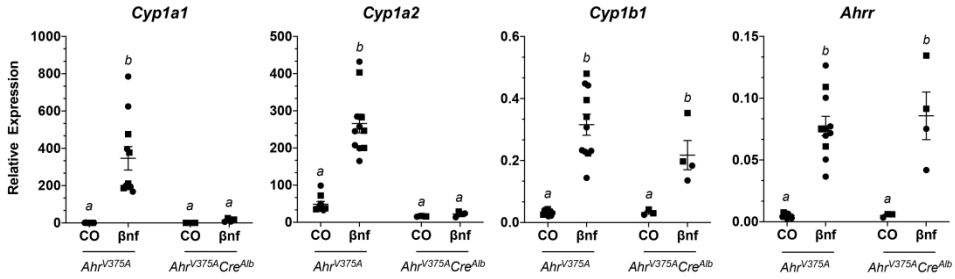

Figure 7. Induction of AHR-driven genes in the high affinity conditional allele excised in hepatocytes (AhrV375ACreAlb). Induction of AHR-driven genes in mice ubiquitously expressing the high affinity conditional allele (AhrGN367R) compared to mice with the AHR excised in hepatocytes (AhrV375ACreAlb). Mice are treated with βNF or corn oil vehicle control (CO) for four hours. Liver mRNA expression of AHR-driven genes relative to Hprt. Groups sharing a superscript are not different at the level of statistical significance ($p > 0.05$). Each point represents the mean of three technical replicates of one biological replicate. Males are represented by a circle while females are represented by a square.

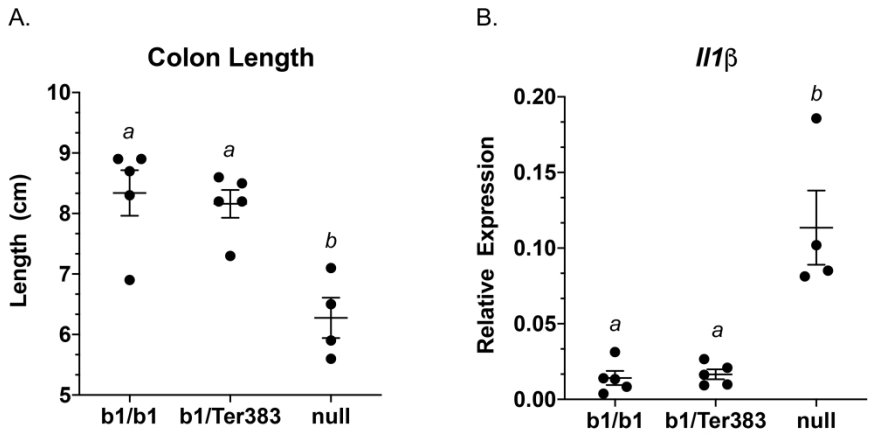

Figure 8. Colitis phenotype in Ahrb1/Ter383 mice. A. Colon length of mice treated with 1% DSS in drinking water for 5 days. Differences between groups sharing a superscript are not statistically significant. B. Relative expression of Il1b and Rorc mRNA transcripts in whole colon of mice treated with 1% DSS in drinking water for 5 days. Differences between groups sharing a superscript are not statistically significant. Each point represents the mean of three technical replicates of one biological replicate.

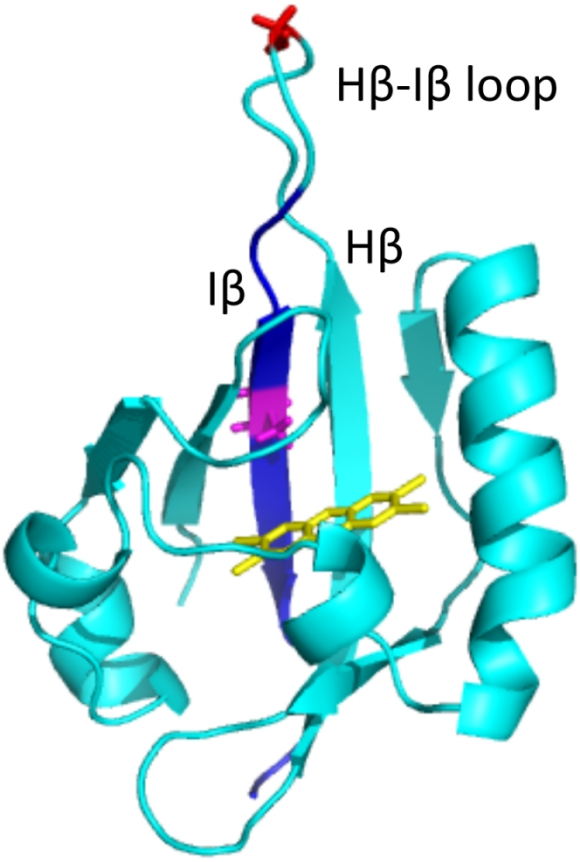

Figure 9. Structural rendition of PAS-B from AHRb1 showing location of amino acids relevant to mutants. The structure of the PAS-B domain modeled from AHRb1 sequence is shown in light blue. A TCDD molecule is shown in the ligand binding pocket in yellow. Residue 375 (Alanine) is highlighted in purple. The Glycine residue at 368 mutated in the AHRNG367R model is highlighted in red, located in the hairpin loop. The residues changed in AHRTer383 are highlighted in dark blue.